# CART Raman Lidar Water Vapor Measurements During the ARM 1996 Water Vapor IOP

*D. D. Turner*
*Pacific Northwest National Laboratory*
*Richland, Washington*

*J.E.M. Goldsmith*
*Sandia National Laboratories*
*Livermore, California*

## Introduction

The first in a series of water vapor intensive operating periods (IOPs) was held during September 1996. These IOPs are designed to address the recognized need, both within and outside the Atmospheric Radiation Measurement (ARM) community, to improve the state-of-the-art in water vapor measurements. The operational Raman lidar system was delivered to the Southern Great Plains (SGP) Cloud and Radiation Testbed (CART) site prior to this IOP, greatly augmenting the water vapor instrumentation at the site.

Due to the nature of this IOP, additional instrumentation was brought to the SGP CART site to provide additional measurements of water vapor and to help characterize the CART instrumentation. In particular, the National Aeronautics and Space Administration (NASA)/Goddard Space Flight Center (GSFC) scanning Raman lidar and the 20.6 GHz microwave radiometer from National Oceanic and Atmospheric Administration's (NOAA's) Environmental Technology Laboratory (ETL) were present and collected data throughout the IOP. To provide redundant in situ measurements, highly accurate temperature and relative humidity sensors from the Oklahoma Mesonet were installed next to the CART tower sensors at 25 and 60 meters. Finally, a tethersonde system from Los Alamos National Laboratory was flown with a chilled mirror device from the surface up to a maximum altitude of 1 kilometer (depending on atmospheric conditions). These instruments, along with some other instruments, complemented the standard CART instruments, which include the CART microwave radiometer (MWR), radiosondes, and in situ tower sensors. This IOP provided an excellent opportunity to calibrate and characterize the CART Raman lidar. The details of the CART Raman lidar system are given by Goldsmith et al. (1995).

## Raman Lidar Calibration

Raman lidar systems detect selected species by measuring the wavelength shifted molecular return produced by Raman scattering from the chosen molecules as a function of time since the laser's pulse. The ratioing of the water vapor and nitrogen return signals provide a profile proportional to the water vapor mixing ratio. To calibrate the Raman lidar system, a scaling factor is derived from comparisons to other measurements of water vapor, which can then be applied to the lidar's ratio profile.

Raman lidar systems tend to operate in the UV, as Raman scattering strength is inversely proportional to the fourth power of the excitation wavelength. During daylight hours, however, the solar background hampers the detection of the weak water vapor Raman signal. The CART Raman lidar uses two operating modes to handle the higher count rates experienced during the daytime periods: a "normal" mode for low background profiling (such as nighttime periods), and a "bright" mode. The two modes differ only by the inclusion of an additional neutral density filter in the water vapor channels when in bright mode. These different modes require that calibration factors be derived for each.

Traditionally, calibration factors for Raman lidar systems have been determined by fitting the lidar's profile to a set of coincident radiosonde profiles. However, recent analyses have shown significant sonde-to-sonde variability (Lesht and Liljegren 1996); hence, it was decided that a different instrument should be used for deriving the calibration factor for the CART Raman lidar. The CART MWR has been at the SGP site for several years and is well characterized (Liljegren and Lesht 1996), so this instrument was chosen as the calibration standard.

Normal mode operation produces water vapor profiles that usually reach up to 9 km, but the bright mode, which is used during high background conditions such as daylight periods, usually does not reach this level. During solar noon, the average height reached by the lidar during the IOP was around 3.5 km, which does not contain all of the precipitable water vapor (PWV) that would be sensed with the MWR. To facilitate the lidar/MWR PWV comparisons, we estimated the fraction of the column sensed by the lidar by interpolating radiosonde profiles to the lidar sample time. We calculated the amount of precipitable water vapor under the maximum limit of the lidar for a given sample, and then calculated the total PWV, both from the interpolated profile. The ratio of these two values provides an estimate of the fraction of the total column sensed by the lidar.

We then proceeded to calibrate both the normal and bright modes by comparing the PWV observed by the lidar (adjusted by the fraction indicated above) with the microwave radiometer. The calibration factors were chosen to minimize the mean square error between the difference of the two instruments' PWV for clear sky cases where the fraction of the column sensed by the lidar was 80% or greater.

# Intercomparison Results

As the CART Raman lidar measures profiles of water vapor, these profiles can be compared to all other water vapor measurements. To this end, the lidar's data was compared to the various other measurements made during the water vapor IOP. Figure 1 provides a snapshot of these results, where the data was separated into two disjoint subsets for analysis based upon the lidar's operating mode (which is a function of the background level).

Detailed analysis of the normal mode results show several results. First, the variability of the radiosonde calibration batches (there were sondes from two batches launched during the IOP) is obvious. Second, there is a small difference between the two Raman lidar systems, even though the NASA/GSFC lidar was also calibrated to the CART MWR. Because the CART lidar operated a higher percentage of the time than did the NASA/GSFC lidar, the CART and NASA/GSFC system were not calibrated with exactly the same sample set of MWR data; hence, the calibration difference. The rather large difference between the chilled mirrors on the tethersonde and the other instruments has yet to be explained. Excellent agreement at the 60-meter level with the in situ sensors was demonstrated in this mode. As the microwave radiometer was used for calibration, we expected perfect agreement. The Bernese GPS intercomparison agrees

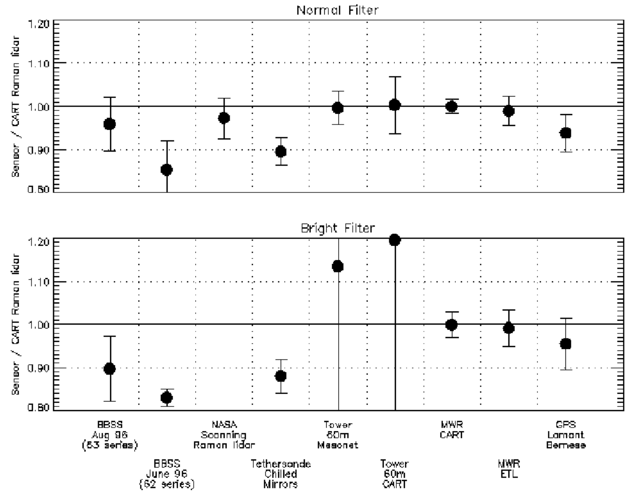


**Figure 1**. Comparisons of different measurements of water vapor with the Raman lidar, for both the normal (nighttime) and bright (daytime) modes. The bars represent one standard deviation.

well, given that the GPS measurement is a hemispheric measurement and the Raman lidar measurement is of the vertical column. Note that the GPS receiver was at Lamont, Oklahoma, not at the CART site.

One of the main features that catches the eye in the bright mode results are the huge error bars for the 60-meter tower comparisons. The explanation is simple: lidar systems have a lower sensitivity near the instrument that increases with altitude to a point before it begins to fall off. This is because the laser beam does not fill the receiver's field of view until the beam is some distance away from the instrument. Therefore, the signal-to-noise level is very low for the first lidar bin. During the night, the low background level does not overwhelm the signal, but during the daytime, the opposite is true; hence, this first bin is quite noisy. New narrower band interference filters have been ordered for the lidar, which should improve its ability near the surface.

An unexpected issue affecting the data quality is the combination of the high background due to the sunlight and the high signal levels. These signals are large enough that they are outside of the linear operating regime of the photon counting system, and thus the output count rate is no longer proportional to the incident light intensity. An effort is underway to perform detector linearity tests described by Donovan et al. (1993) to optimize the linear regime and increase the lidar's dynamic range. It should be noted that this problem affects the normal mode data during sunrise/sunset, when the background levels are starting to rise/fall, as well as the bright mode data. All normal mode results shown here have had the sunrise/sunset periods removed from the analysis.

A lot of detail is lost when distilling the information for Figure 1. A more detailed analysis was performed for the lidar and the CART MWR. These results are shown in Figure 2. While there is high correlation between the two different measurements, a nonzero intercept together with a non-unity slope are still under investigation. The error due to the high background levels can be seen in the bright mode data, causing the difference in slope as compared to the normal mode data. It should again be noted that the CART MWR was used to derive the calibration factor for the CART Raman lidar. Comparisons with the ETL MWR show similar results.

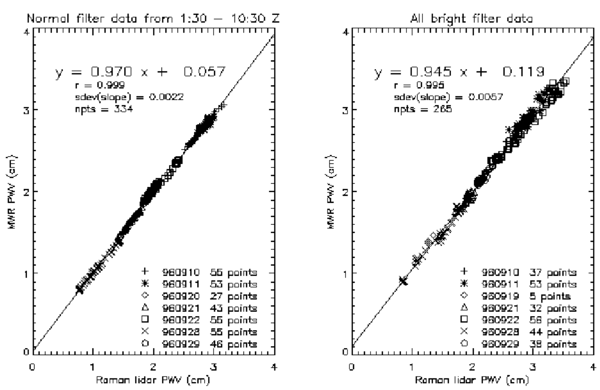


**Figure 2**. Scatterplot of the total precipitable water measured by the Raman lidar and the microwave radiometer. Cloudy samples and samples where the lidar sensed less than 80% of the total column are excluded. Note that for samples where the lidar sensed between 80% - 99% of the total column, the PWV from the lidar has been adjusted accordingly. See the text for details.

A similar analysis was done with the high quality "Mesonet" sensors that were mounted on the 60-meter tower at the CART site. Using the first bin from the low (wide field of view) channel from the lidar, we again see a non-unity slope for the normal mode data in Figure 3. The high noise level in the bright mode data is easily seen in this figure.

Analysis of the vertical profiles measured by the CART lidar was done, comparing these to those measured by the two batches of radiosondes and the NASA/GSFC Raman lidar. These results are shown in Figures 4 and 5. It should be noted that the CART lidar agrees well in altitude (calibration aside)

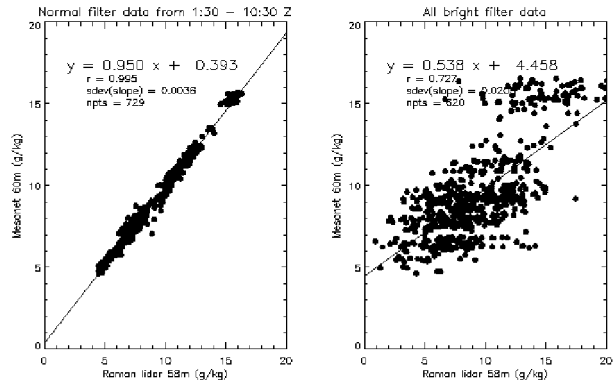


**Figure 3**. Scatterplot of the mixing ratio at 60 meters from the Raman lidar and the "Mesonet" sensors placed on the 60-meter tower.

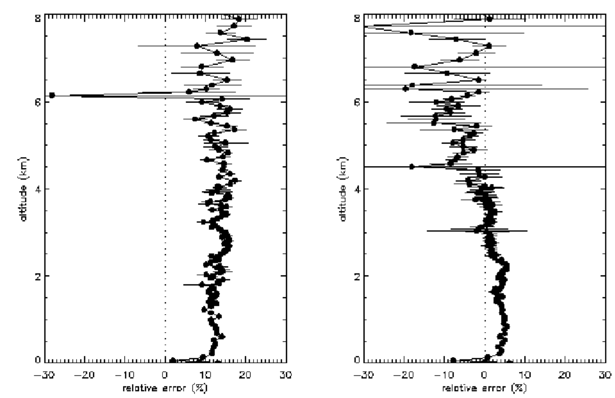


**Figure 4**. Mean error profiles from the two batches of radiosondes with respect to the Raman lidar. These are the normal mode results. The sonde batch calibrated in June 1996 is on the left, the August 1996 calibrated batch on the right.

with the sondes calibrated in June 1996, while the NASA/GSFC lidar agrees with the August calibrated sondes with altitude. Note that only normal mode data was used in this study. These differences in altitude are still under investigation.

# Conclusion

The water vapor IOP brought together an impressive amount of state-of-the-art instrumentation for the purposes of understanding the capabilities of each and furthering the state-of-the-art in this area. While the overall results demonstrated excellent agreement between the wide variety of measurement techniques, some questions are still unanswered. However,

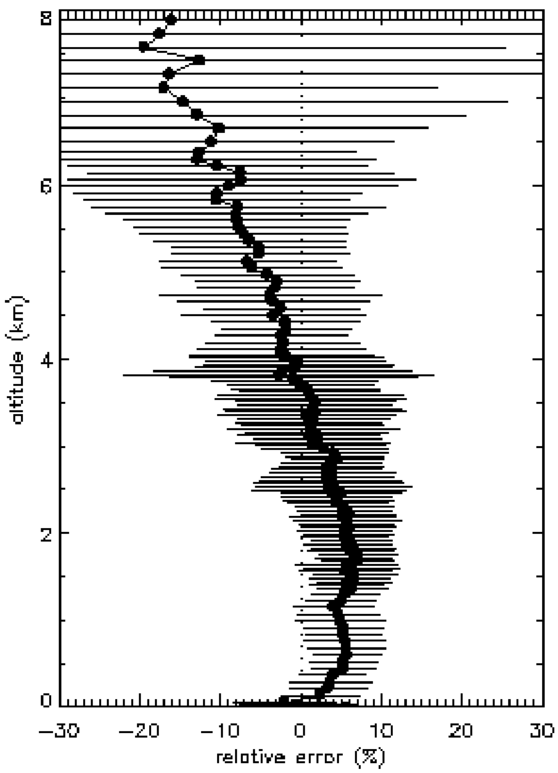


**Figure 5**. Mean error profile from the NASA/GSFC Raman lidar with respect to the CART Raman lidar.

the CART Raman lidar system has proved to be a valuable addition to the SGP CART site, running over 65% of the IOP, with most of the down time due to inclement weather (there were no mechanical failures). This ruggedized system, capable of high-resolution profiling of water vapor, can be used to improve all of the CART water vapor measurements and provide a valuable supply of vertical distribution data that was previously unattainable with radiosondes. With the recent installation of a hail shield to protect the window from inclement weather, the CART Raman lidar is now operating routinely 24 hours a day, supplying the SGP CART site with high temporal and vertical resolution water vapor data at a level that used to be restricted only to IOPs.

## References

Donovan, D. P., J. A. Whiteway, and A. I. Caswell, 1993: Correction for nonlinear photon-counting effects in lidar systems. *Appl. Optics*, **32**, (33).

Goldsmith, J.E.M., F. H. Blair, and S. E. Bisson, 1995: Implementation of Raman lidar for profiling of atmospheric water vapor and aerosols at the Southern Great Plains (SGP) Cloud and Radiation Testbed (CART) site. *Proceedings of the Fifth Atmospheric Radiation Measurement (ARM) Science Team Meeting*, CONF-9503140.

Lesht, B. M, and J. C. Liljegren, 1996: Comparison of precipitable water vapor measurements obtained by microwave radiometry and radiosondes at the Southern Great Plains CART site. *Proceedings of the Sixth Atmospheric Radiation Measurement (ARM) Science Team Meeting*, CONF-9603149.

Liljegren, J. C., and B. M. Lesht, 1996: Measurements of integrated water vapor and cloud liquid water from microwave radiometers at the DOE ARM cloud and radiation testbed in the U.S. southern great plains. *Proceedings of the International Geoscience and Remote Sensing Symposium (IGARSS).*